View Article Online
View Journal

Dalton Transactions

An international journal of inorganic chemistry

Accepted Manuscript

This article can be cited before page numbers have been issued, to do this please use: A. Borah, S. Dey, S. K. Gupta, G. Rajaraman and R. Murugavel, *Dalton Trans.*, 2023, DOI: 10.1039/D3DT01206A.

This is an Accepted Manuscript, which has been through the Royal Society of Chemistry peer review process and has been accepted for publication.

Accepted Manuscripts are published online shortly after acceptance, before technical editing, formatting and proof reading. Using this free service, authors can make their results available to the community, in citable form, before we publish the edited article. We will replace this Accepted Manuscript with the edited and formatted Advance Article as soon as it is available.

You can find more information about Accepted Manuscripts in the Information for Authors.

Please note that technical editing may introduce minor changes to the text and/or graphics, which may alter content. The journal's standard Terms & Conditions and the Ethical guidelines still apply. In no event shall the Royal Society of Chemistry be held responsible for any errors or omissions in this Accepted Manuscript or any consequences arising from the use of any information it contains.

ROYAL SOCIETY OF CHEMISTRY

rsc.li/dalton

DOI: 10.1039/D3DT01206A

Field-Induced SIM Behaviour in Early Lanthanide(III) Organophosphates Incorporating 18-crown-6

Aditya Borah, Sourav Dey, Sandeep K. Gupta, Gopalan Rajaraman and Ramaswamy Murugavel*

Department of Chemistry, Indian Institute of Technology, Powai, Mumbai
*Corresponding author; email: rmv@chem.iitb.ac.in

ABSTRACT

Single-ion magnets (SIMs) have attracted wide attention in recent years. Despite tremendous progress on late lanthanide SIMs, report on early lanthanide exhibiting SIM characteristics is scarce. A series of five novel 18-crown-6 encapsulated mononuclear early lanthanide(III) organophosphates, [{(18-crown-6)Ln(dippH)$_3$}{(18-crown-6)Ln(dippH)$_2$(dippH$_2$)}]·[I$_3$] [Ln= Ce (**1**), Pr (**2**), Nd (**3**)] and [{Ln(18-crown-6)(dippH)$_2$(H$_2$O)}·{I$_3$}], [Ln= Sm (**4**) and Eu (**5**)] have been synthesised in the present study. 18-crown-6 coordinates to Ln(III) ions in an approximate equatorial position while the axial positions are occupied either by three phosphate moieties in **1-3** or two phosphate moieties and one water molecule in **4** and **5**, resulting in a muffin-shaped coordination geometry around the Ln(III) centres. Magnetic susceptibility measurements reveal that Ce and Nd complexes as field-induced single-ion magnets with significant barrier heights. Furthermore, the ab initio CASSCF/RASSI-SO/SINGLE_ANISO calculations on complexes **1** and **3** reveal significant QTM in the ground state rationalising the field-induced single-ion magnetism behaviour of these complexes.

DOI: 10.1039/D3DT01206A

Introduction

We live in an era where a large amount of information is stored in electronic form. These data are saved in the conventional devices where the binary language (1 and 0; called bit information unit) is employed. Unfortunately, the development of data storage devices cannot meet the rate of exponential production of the data, due to different factors such as dimensions of the nanoparticle used, limited thermal activation barriers and smaller blocking-temperature. Singe-molecule magnets (SMMs)[1] can be an alternative and better option in this context as they provide the opportunity to store data at the molecular level, which can reduce the size of the devices by at least ten times. SMMs are molecules with a bistable ground spin state exhibiting slow relaxation of magnetisation below the blocking temperature (T_B). The work of Donati *et al.*, on storing data in single holmium atoms adsorbed on a magnesium oxide film grown on a silver substrate, proved that it is possible to store data even at an atomic level.[2-3] At the molecular level, the strategy of designing high-performing SMMs has shifted from clusters to mononuclear complexes, known as single-ion magnets (SIMs).[4-6] A high-performing SMM is characterised by two parameters namely the barrier height of spin reversal (U_{eff}) and blocking temperature (T_B). In the past two decades, trivalent lanthanide(III) ions based SIMs have gained unprecedented interest, over the transition metal ion SIMs, due to their strong spin–orbit coupling as well as large intrinsic magnetic anisotropy. Among Ln(III) ions, the oblate-shaped Dy(III) based SIMs are leading the race in achieving higher T_B that surpasses liquid nitrogen temperature (80 K).[3, 7-24] In the context of designing single-ion magnets, late Ln(III) ions, such as Dy(III), Er(III) and Tb(III), have been heavily explored while early Ln(III) ions are scarcely studied due to smaller magnetic momentum (J = L-S) and weaker spin-orbit coupling.[25-27] Interestingly, lighter lanthanides, especially samarium and neodymium, are used in classical hard magnets for industrial use (e.g. $SmCo_5$ and $Nd_2Fe_{14}B$).[28] Moreover, the magnetic properties of $Nd_2Fe_{14}B$ can be enhanced by doping such as dysprosium(III) and cerium(III) ions .[29] Thus, early Ln(III) ions also have the potential to exhibit SIM behaviour.

With the rapid progress of this field, it is convincible that designing a suitable ligand field (LF) for a given metal ion is the most crucial task: an axially stressed LF is best for oblate-shaped Ln(III) ions while equatorially stressed LF is for prolate-shaped Ln(III) ions.[30] On placing a Ln(III) ion in a suitable LF, the inherent magnetic anisotropy can be enhanced to a large extent. Being oblate, Ce(III) ion (configuration: f^1; ground state: $^2F_{5/2}$) requires an axially stressed LF, where the six-fold degenerate ground state is split into three sets of Kramers pairs, $|J_z|$ = 5/2, 3/2, and 1/2, where J_z sublevels with higher electron density along z axis (e.g. $|J_z|$ =1/2) are destabilised more than $|J_z|$=5/2 sublevels.[31] To realise an easy axis anisotropy, other oblate shaped early Ln(III) ions, such as Pr(III), Nd(III) etc., also need the same strategy as Ce(III) ion. Employing such a strategy, a number of Ce and Nd ion based singe-ion magnets have been successfully designed (Tables 1 and 2).

The selective metal encapsulation chemistry of crown ethers (e.g.: Li^+ in 12-crown-4, Na^+ in 15-crown-5, and K^+ in 18-crown-6 etc.), due to their precise cavity size with the metal ions, offers an opportunity for axially stressed C_n (n=4, 5, 6) symmetric LF. Like K^+, the Ln(III) ions are the best fit for the cavity of 18-crown-6, while in the case of smaller crown ethers, Ln(III) ions sit out of the cavity. As crown ether oxygen ceters interact only weakly with the Ln(III) centres, a ligand field comprising of strong axial ligands and weak equatorial 18-crown-6[32-34] would be expected the ideal strategy for designing high-performance SIMs derived from oblate lanthanides.[33-38]

Based on these earlier observations and building up on our recent results on phosphorus ligand based SIMs,[39-42] we report here a series of early Ln(III) (Ln: Ce, Pr, Nd, Sm and Eu) organophosphate complexes [{(18-crown-6)Ln(dippH)$_3$}{(18-crown-6)Ln(dippH)$_2$(dippH$_2$)}]·[I_3] [Ln= Ce (**1**), Pr (**2**), Nd (**3**)] and [{Ln(18-crown-6)(dippH)$_2$(H_2O)}·{I_3}], [Ln= Sm (**4**) and Eu (**5**)], derived from 2,6-diisopropylphenylphosphates (dippH$_2$) as axial ligands, incorporating 18-crown-6 ligand in the equatorial positions. Hexadentate18-crown-6 produces a pseudo hexagonal equatorial plane around the Ln(III) centre. A number of oblate-shaped Ln(III) ion (specially Dy(III) ion) based single-ion magnets with hexagonal equatorial plane are found to have significantly high barrier heights of spin reversal.[32-33, 43-48] Such complexes with local hexagonal bipyramidal geometry fulfill the strong magnetic axiality and high coordination number providing the air stability to the complexes.

Table 1. Ce(III) based single-ion magnets ($U_{eff,ac}$ represents the barrier obtained from ac susceptibility measurements; $U_{eff,Cal}$ represents the barrier obtained from computational studies, C and n are the parameters obtained from the fitting of temperature dependence of relaxation time plot using Raman process):

Sl no.	Ce(III) SIMs	C.N.*	*Orbach Process*			*QTM*	*Raman*		H / Oe	Ref
			$U_{eff,ac}$ / K	τ_0 / s	$U_{eff,ca}$ / K	τ_{QTM} / s	C $/s^{-1}K^{-n}$	n		
1	Compound **1**	9	16.4 16.3	6.0×10^{-5} 2.2×10^{-6}	671	0.079 0.0025	–	–	350	This work
2	$Li(DME)_3[Ce^{III}(COT'')_2]$	16 (η^8)	30	1.2×10^{-6}	–	–	–	–	400	[49]
3	$[Ce(NO_3)_3(18\text{-crown-}6)]$	12	31.4 30.3	1.8×10^{-7} 2.3×10^{-7}	– –	– –	– 0.108	– 5	1000	[34]
4	$[Ce(NO_3)_3(1,10\text{-diaza-}18\text{-crown-}6)]$	12	44 44	2.3×10^{-8} 2.6×10^{-7}	– –	– –	– 0.52	– 5	1000	[34]
5	$[Ce(NO_3)_3(HL^1)_3]$	12	37.5	2.76×10^{-8}	501	0.076	0.154	7.36	3000	[50]
6	$Ce(fdh)_3(bpy)$	8	33.3	1.8×10^{-7}	-	–	0.40	6	2000	[51]
7	$[Ce(NO_3)_3L^2_3]$	9	21.5 –	2.7×10^{-7} –	317	– –	– 1.44	– 6.8	200 200	[52]
8	$[Ce(ntfa)_3(MeOH)_2]$	8	46.4	8.13×10^{-10}	460	–	–	2.98	200	[53]
9	$[Ce(ntfa)_3(5,5'\text{-}Me_2bipy)]$	8	13.6	3.53×10^{-6}	371	–	–	8.01	200	[53]
10	$[Ce(ntfa)_3(bpy)_2]$	8	22.7	1.61×10^{-6}	468	–	–	1.28	200	[53]
11	$[Ce(dppbO_2)_2Cl_3]$	6	54	2×10^{-10}	420	–	31	3.4	100	[54]

Where, COT'': bis(trimethylsilyl)cyclooctatetraenyl dianion; HL^1= 2-methoxy-6-[(E)-phenylimino-methyl]phenol; fdh: 1,1,1-fluoro-5,5-dimethyl-hexa-2,4-dione; bpy: 2, 2′-bipyridine; L^2: ^{t}BuP(O)(NH^iPr)$_2$; Ntfa: 4,4,4-trifluoro-1-(naphthalen-2-yl)butane-1,3-dionato, $5,5'\text{-}Me_2bipy$: 5,5′-dimethyl-2,2′-dipyridyl; $dppbO_2$: 1,2-bis(diphenylphosphino)benzene dioxide; *C.N. = coordination number

Table 2. Nd(III) based single-ion magnets ($U_{eff,ac}$ represents the barrier obtained from ac susceptibility measurements; $U_{eff,Cal}$ represents the barrier obtained from computational studies, C and n are the parameters obtained from the fitting of the temperature dependence of relaxation time plot using Raman process):

Sl no.	*Nd(III) SIMs*	*C.N.**	$U_{eff,ac}$ / K	τ_0 / s	$U_{eff,cal}$ / K	τ_{QTM} /s	*C* $/s^{-1}\ K^{-n}$	*n*	H/Oe	Ref
1	Compound **3**	***9***	***6***	1.0×10^{-5}	259	–	501	3	1500	This work
2	$[NdTp_3]$	9	4	2.6×10^{-4}	165	-	-		100	[55]
3	$[Li(DME)_3][Nd^{III}(COT'')_2]$	16 (η^8)	21	5.5×10^{-5}	-	-	-	-	1000	[56]
4	$[Nd(NO_3)_3(18\text{-crown-}6)]$	12	29.9 30.9	2.9×10^{-9} 2.2×10^{-9}	-	- -	- 4.1	- 5	1000 1000	[34]
5	$[Nd(NO_3)_3(1,10\text{-diaza-}18\text{-crown-}6)]$	12	69 73	2.1×10^{-10} 1.4×10^{-10}	- -	- -	- 0.00107	- 9	1000 1000	[34]
6	$[Nd(NO_3)_2L^3]PF_6.MeCN$	10	36	4.4×10^{-9}	-	-	2.8	5	1000	[57]

7	$[L_2Nd(H_2O)_5][I]_3 \cdot L^1_2 \cdot (H_2O)$	7	16.1 24.7 39.2	2.6×10^{-4} 5.0×10^{-6} 8.9×10^{-7}	302	0.001	4.2×10^{-18} 0.0292	5 5	0 0 2000	58
8	$[Nd(CyPh_2PO)_2(H_2O)_5]I_3 \cdot 2(CyPh_2PO) \cdot 3EtOH$	7	-	-		0.005	-	5.12 6.54	0 2000	59
9	$[Cp^*_2Nd(BPh_4)]$	10	41.7	1.4×10^{-6}		-	0.0286	5.2	1000	60
10	$[Nd^{III}(TTA)_3(MeOH)_2]) \cdot 0.5A$ zo-py) Before heating After heating	8	 19.7 27.3	 3.8×10^{-7} 8.5×10^{-8}		 0.008 -	 - -	 -	 1000	61
11	C_1 symmetric $[C(NH_2)_3]_5[Nd(CO_3)_4(H_2O)] \cdot 2$ H_2O	9	30.7	1.1×10^{-7}		-	0.89	6.08	1500 1500	62
12	C_4 symmetric $[C(NH_2)_3]_4[H_3O][Nd(CO_3)_4(H$ $O)] \cdot 9.5H_2O$	9	9.25	2.1×10^{-6}		-	413.85	3.63	1500	62

Where, Tp^-: trispyrazolylborate; L^3: a single helical hexadentate Schiff base ligand; TTA= thenoyl(trifluoro)acetonate and Azo-py = 4,4′-azopyridine; and *C.N. = coordination number

Experimental Section

Instruments and Methods: All the reactions were performed at ambient reaction conditions. Fourier-transform infrared spectra were recorded on a Perkin Elmer Spectrum One spectrometer using KBr diluted pellets. Microanalyses were performed on a Thermo Finnigan (FLASH EA 1112) microanalyser. Powder X-ray diffractions were recorded on a Philips X'pert Pro (PANalytical) diffractometer using Cu Kα radiation (λ = 1.54190 Å). The magnetic properties of the polycrystalline samples were measured using a Quantum Design MPMS-XL SQUID magnetometer equipped with a 7 T magnet in the temperature range 2-300 K. The data were corrected for the background contribution and consequently the Pascal's constants. Alternating current (ac) susceptibility measurements were performed with an oscillating ac field of 3.5 Oe oscillating at indicated frequencies between 0.1 and 1500 Hz.

Materials: Commercial grade solvents were purified by employing conventional procedures.[63] Lanthanide iodides were prepared from Ln(III) oxides and Hydriodic acid. 2,6-Diisopropylphenol and phosphorous oxychloride were procured from commercial sources and used as received. 2,6-Diisopropylphenyl phosphate was synthesised as described previously in the literature.[64]

General procedure for the synthesis of compounds 1-5. To the solution of hydrated $LnI_3.xH_2O$, (Ln= Ce(**1**), Pr(**2**), Nd(**3**), Sm(**4**) and Eu(**5**) (0.1 mmol) in ethanol (5 mL), 18-crown-6 (0.2 mmol, 53 mg) was added and stirred for an hour at room temperature, which produces a dark brown precipitate. To this reaction mixture, methanol (10 mL) is added and stirred till the solution becomes clear yellow. A solution of 2,6-diisopropylphenylphosphate (0.3 mmol, 77.5 mg) in methanol (5 mL) was added into it and stirred for 2 hours at 60 ^oC and then cooled to room temperature. The reaction mixture was filtered and the resultant yellow clear solution was left for crystallisation at ambient temperature through slow evapoaration of the solvent to yield the respective metal phosphats as block shaped reddish-brown crystals after 1 week.

Characterisation of [{(18-crown-6)Ce(dippH)$_3$}{(18-crown-6)Ce(dippH)$_2$(dippH$_2$)}]·[I$_3$] (1): m.p. > 250 ^oC ; FTIR (KBr, cm^{-1}): 3061 (w), 2961 (s), 2868 (m), 2356 (br), 1667 (br), 1466 (s), 1439 (s), 1382 (m), 1352 (m),1335 (s), 1255 (s), 1173 (s), 1091 (vs), 1046 (m), 964 (s), 944 (s), 912 (m), 880 (m), 840 (m), 799 (m), 769 (s), 746 (m), 660 (m), 592 (m), 548 (s), 513 (s); Anal. Found (Calculated) for $C_{96}H_{155}I_3O_{36}P_6Ce_2$: C, 41.97 (42.20); H, 5.57 (5.72).

Characterisation of [{(18-crown-6)Pr(dippH)$_3$}{(18-crown-6)Pr(dippH)$_2$(dippH$_2$)}]·[I$_3$] (2): m.p. > 250 ^oC; FTIR (KBr, cm^{-1}): 3062 (w), 2964 (s), 2868 (m), 2358 (br), 1658 (br), 1466 (s), 1439 (s), 1383(m), 1352 (m),1335 (s), 1255 (s), 1175 (s), 1090 (vs), 1047 (m), 963 (s), 940 (s), 908 (m), 881 (m), 840 (m), 799 (m), 764 (s), 744 (m), 655 (m), 593 (m), 540 (s), 514 (s); Anal. Found (Calculated) for $C_{96}H_{155}I_3O_{36}P_6Pr_2$: C, 41.96 (42.11); H, 5.93 (5.71).

Characterisation of [{(18-crown-6)Nd(dippH)$_3$}{(18-crown-6)Nd(dippH)$_2$(dippH$_2$)}]·[I$_3$] (3): m.p. > 250 °C; FTIR (KBr, cm^{-1}): 3065 (w), 2959 (s), 2868 (m), 2357 (br), 1626 (br), 1467 (s), 1445 (s), 1383(m), 1349 (m),1333 (s), 1252 (s), 1176 (s), 1103 (vs), 1084 (s), 960 (s), 883 (m), 835 (m), 803 (m), 770 (s), 749 (m), 661 (m), 594 (m), 542 (s), 514 (s); Anal. Found (Calculated) for $C_{96}H_{155}I_3O_{36}P_6Nd_2$: C, 42.09 (42.08) ; H, 5.54 (5.70).

Characterisation of [{Sm(18-crown-6)(dippH)$_2$(H$_2$O)}·{I$_3$}] (4): m.p. > 250 °C; FTIR (KBr, cm^{-1}): 3065 (w), 2964 (s), 2869 (m), 2355 (br), 1624 (br), 1466 (s), 1442 (s), 1384(m), 1362 (m), 1350 (m), 1334 (s), 1256 (s), 1178 (vs), 1105 (vs), 1084 (s), 959 (vs), 835 (m), 799 (m), 770 (s), 749 (m), 662 (m), 593 (m), 538 (s), 513 (s); Anal. Found (Calculated) for $C_{48}H_{79}I_3O_{18}P_3Sm_1$: C, 32.78 (33.01); H, 4.69 (4.62).

Characterisation of [{Eu(18-crown-6)(dippH)$_2$(H$_2$O)}·{I$_3$}] (5): m.p. > 250 °C; FTIR (KBr, cm^{-1}): 3078 (w), 2952 (s), 2867 (m), 2348 (br), 1626 (br), 1466 (s), 1445 (s), 1383 (m), 1350 (m), 1332 (s), 1253 (s), 1176 (vs), 1105 (vs), 1083 (s), 961 (vs), 836 (m), 805 (m), 771 (s), 750 (m), 661 (m), 595 (m), 545 (s), 514 (s); Anal. Found (Calculated) for $C_{48}H_{79}I_3O_{18}P_3Eu_1$: C, 32.26 (32.52); H, 4.79 (4.70).

Single crystal X-ray crystallography: Single crystals of **1**-**5** suitable for diffraction studies were selected under an optical microscope and mounted on a Rigaku Saturn 724+ CCD diffractometer for unit cell determination and intensity data collection. Data integration and indexing were carried out using CrysAlisPro software. Using Olex software[65], the structure was solved with the ShelXT[66] structure solution program using Intrinsic Phasing. The complete refinement of the structures was carried out with the ShelXL[67] refinement package using Least Squares minimisation. All non-hydrogen atoms were refined anisotropically. The hydrogen atoms were refined isotropically as rigid atoms.The frequency dependent ac susceptibility plots, cole-cole plots and 1/τ vs 1/T plots are fitted with CC-FIT2 software[68].

Computational Details: The ab initio calculations were performed using MOLCAS 8.2 program package using the atomic position obtained from X-ray structure. The anions were excluded from the calculations. The basis set for our calculations was taken from the ANO-RCC library as implemented in the MOLCAS program package. We have used the following basis sets in our calculations; [Ce.ANO-RCC...8s7p5d3f2g1h.] for Ce, [Nd.ANO-RCC...8s7p5d3f2g1h.] for Nd, [P.ANO-RCC...4s3p1d.] for P, [O.ANO-RCC...3s2p1d.] for O, [C.ANO-RCC...3s2p.] for C and [H.ANO-RCC...2s.] for H. The Douglas-Kroll-Hess (DKH) Hamiltonian was employed to take into account the scaler relativistic effect. The disk space of our calculations was reduced by the Cholesky decomposition technique. The spin-free states of complexes **1** and **3** were generated by CASSCF (complete active space self-consistent field) method with CAS(1,7) and CAS(3,7) active space, respectively. Within this active space, we have computed the energies of 7 doublets for **1** and 35 quartets and 112 doublets for **3**. The spin-orbit coupling between these spin-free states was considered perturbatively by the restricted active space state interaction (RASSI) method. We have not performed CASPT2 calculations due to the dominant ionic character of the Ln-ligand bond. Finally, the g tensor, magnetic moment, QTM/TA-QTM, blocking barrier etc., were computed from the SINGLE_ANISO module of MOLCAS.

Results and Discussion

Synthetic aspects: Considering the perfect fitting of Ln(III) ions in the void of 18-crown-6 as well as oxophilicity nature of Ln(III) ions, an organophosphate monoester (2,6-diisopropylphenylphosphate, dippH$_2$) and 18-crown-6 are used to design a suitable ligand field around the mentioned early Ln(III) ions. Fully deprotonated organophosphates (ArOPO$_3^{2-}$) generally act as polydentate ligands which produce either polynuclear clusters or polymers.[39-40] Such polymerisation is controlled in this work by stopping dippH$_2$ from fully deprotonation, by carrying out the reaction in the absence of any base. This strategy successfully yields mononuclear 18-crown-6 ether encapsulated Ln(III) organophosphates. The reactions between LnI$_3$.xH$_2$O, 18-crown-6 and dippH$_2$ (1:2:3) were carried out at 60 °C in a solvent-mixture of ethanol and methanol (Scheme-1). On evaporation of the reaction mixture, compounds **1-5** are obtained as air-stable blocked shaped reddish-brown crystals within a period of 1-2 weeks. All the five compounds were characterised by means of different analytical and spectroscopic techniques. Further, the molecular structures of all the molecules are have been established by the single crystal X-ray diffraction studies. The phase purity of all the complexes is confirmed with the help of powder X-Ray diffraction studies on polycrystalline samples.

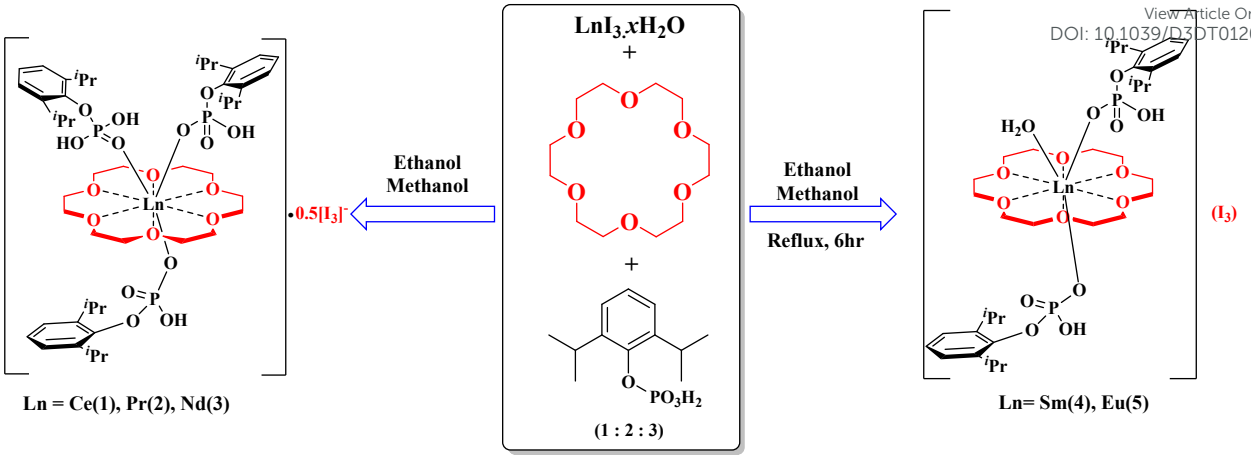

Scheme-1: General synthetic scheme of **1-5**

Molecular structure of 1-3: Slow evaporation of the respective reaction mixtures from the reaction between respective hydrated Ln(III) iodides, 18-crown-6 and $dippH_2$ in a solvent mixture of methanol and ethanol yield air-stable reddish-brown coloured good quality crystals under ambient conditions. Single crystal X-ray diffraction studies reveal that all the three mononuclear complexes crystallise in a triclinic space group $P\bar{1}$, (**1** and **2** are isostructural).

In all the three cases, Ln(III) centre fits perfectly at the void of 18-crown-6 and thus it wraps the Ln(III) ions through the equatorial plane in a non-planar fashion, as all the atoms of the crown are sp^3 hybridised (figure 1b, 1c). The three monocoordinated organophosphate ligands coordinate to the Ln(III) centre through axial positions in "Y" fashion. The lattice triiodide ion is present at the centre of inversion, which is shared by two symmetrically equivalent Ln-moeities. Thus, the asymmetric unit has half of I_3^- ion along with one Ln complex. Thus, the full molecule of this class can be represented as $[\{(18\text{-crown-6})Ln(dippH)_3\}\{(18\text{-crown-6})Ln(dippH)_2(dippH_2)\}]\cdot[I_3]$ (Ln: Ce(**1**), Pr(**2**) and Nd(**3**)). The asymmetric unit and molecular structure of **1** is shown as representative example of **1-3**. The asymmetric units and molecular strutures of **2** and **3** are also shown in figure S3 and S5. The average axial Ln-O(P) bond distances are shorter as compared to the average equatorial Ln-O(crown) distances in **1-3** (Table-3), expecting an axially stressed ligand field around the metal centres. Such an axially stressed ligand field is suitable for all the three Ln(III) ions (Ce(III), Pr(III) and Nd(III) as they possess oblate-shaped f-electron cloud. The selected bond lengths and bond angles of **1-3** are listed in table S1-S3 respectively.

View Article Online
DOI: 10.1039/D3DT01206A

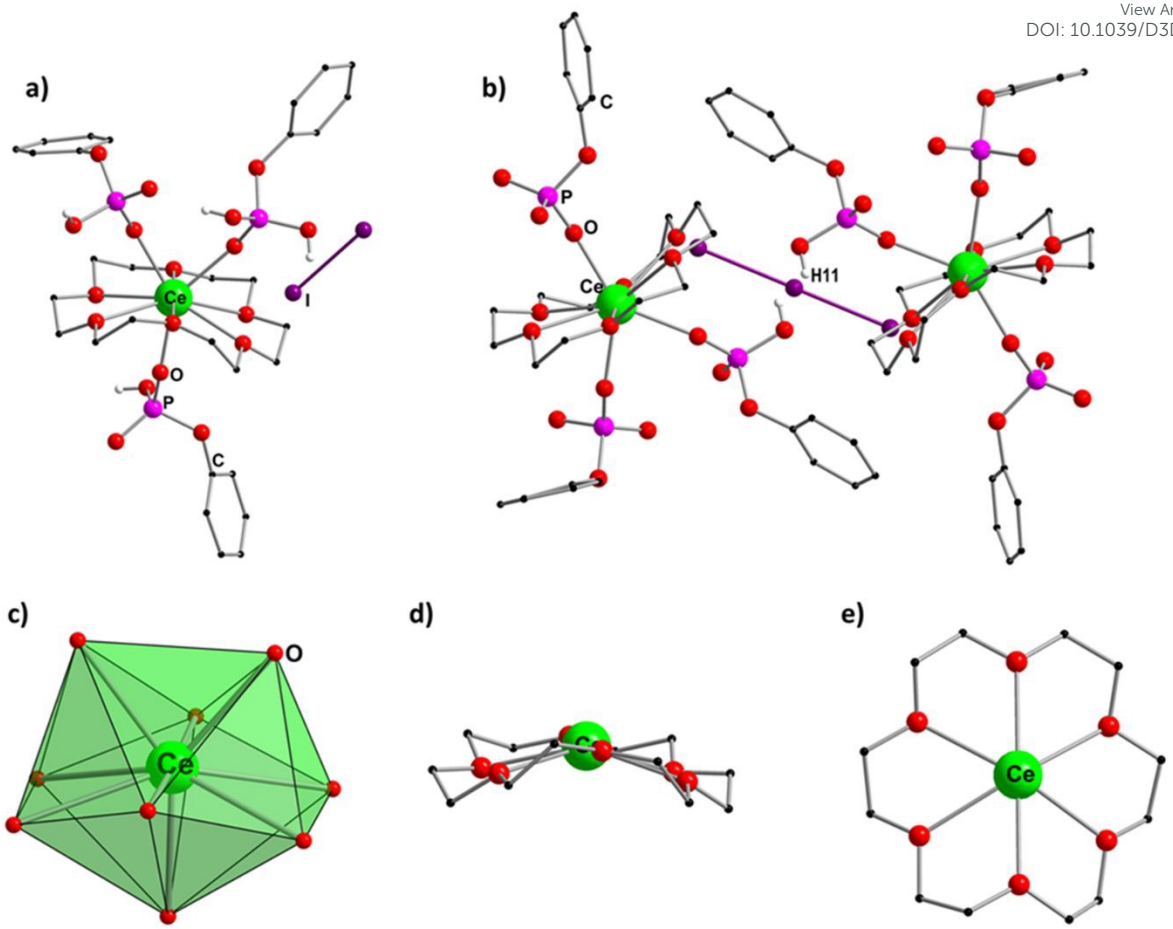

Figure 1. Molecular structure of **1**. (a) The asymmetric unit and (b) full molecule of **1**. (c) Muffin shaped coordination polyhedra around the nine-coordinated Ce(III) ion. (d) The side view and (e) top view of the binding mode of 18-crown-6 to Ce(III) centre, coordinates in a wavy fashion. The hydrogen atoms (except H11 present in the spatial position) and the solvent molecules are omitted for clarity. The coordination mode of 18-crown-6 and muffin shaped cordiantion polyhedra are same for all the three complexes, hence those of **1** are shown as representative case.

Molecular structure of 4 and 5: By employing the same reaction strategy of **1-3**, reddish brown coloured crystals of **4** and **5** were obtained by slow evaporation of the solvent from the reaction mixture. The solid-state structures of both the complexes determined by single-crystal X-ray diffraction studies reveal that both **4** and **5** are mononuclear complexes, crystallise in triclinic $P\bar{1}$ space group. The asymmetric unit of **4** contains one complete molecule of **4** along with one I_3^- anion and one water molecule in the lattice. The asymmetric unit of **5** has two complete molecules along with two I_3^- anions, along with lattice ethanol molecule in the lattice. The molecular structure of **5** is shown in Figure 2a. The core structure of **4** and **5** are slightly different from **1-3**. Instead of three axial arylphosphates in **1-3**, in case of **4** and **5**, two arylphosphates along with one water molecule occupy the three axial positions. Despite the fact that the same stoichiometry of metal and ligand was maintained (metal:ligand = 1:3) throughout the synthesis of all the five complexes, the resultant products have significant differences in the coordination environment. This can be attributed to the relatively smaller size of Sm(III) and Eu(III) as compared to Ce(III), Pr(III) and Nd(III). The smaller size prevents the third arylphosphate moiety from binding to the metal centres in **4** and **5**. Both the arylphosphates are mono-deprotonated ($dippH^-$) and the triiodide ion present in the lattice maintains the charge neutrality.

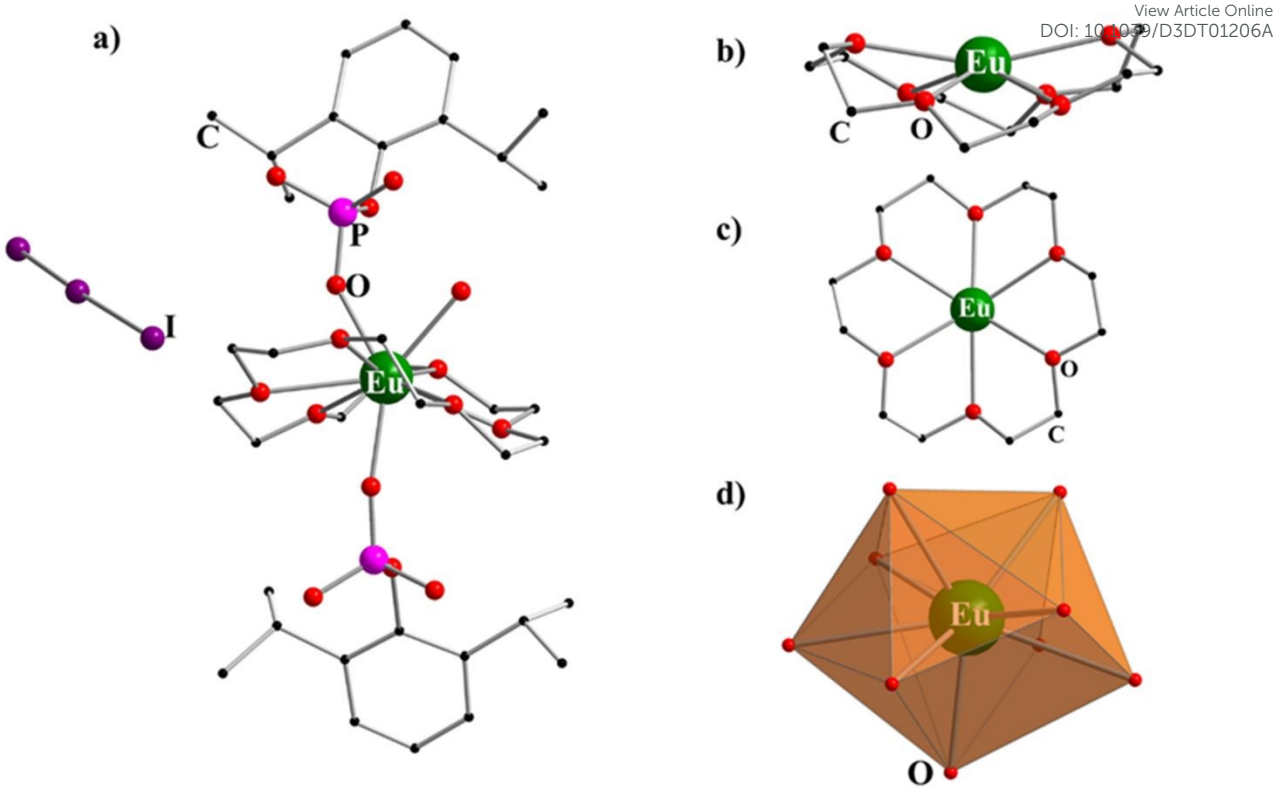

Figure 2. (a) Molecular structure of **5**. The hydrogen atoms and the solvent molecules are omitted for clarity. (b) The side view and (c) the top view of the binding mode of 18-crown-6 to the Eu(III) centre, coordinates in a wavy fashion. (d) The coordination environment of nine-coordinated Eu(III) ion. The molecular structure of **4** is added in ESI.

Due to the presence of bulky organophosphate ligands, the cyclic crown ethers, large triiodide ions and the other lattice solvent molecules facilitate the long separation of the Ln(III) ions, ranging from 9.8 to 10.8 Å (Table S7). The lattice arrangement in **2** and **5** are depicted in figure 3 (See ESI for **1, 3** and **4**). The large distance between any two Ln(III) ions reduces the probalilty of any intermolecular magnetic interactions.

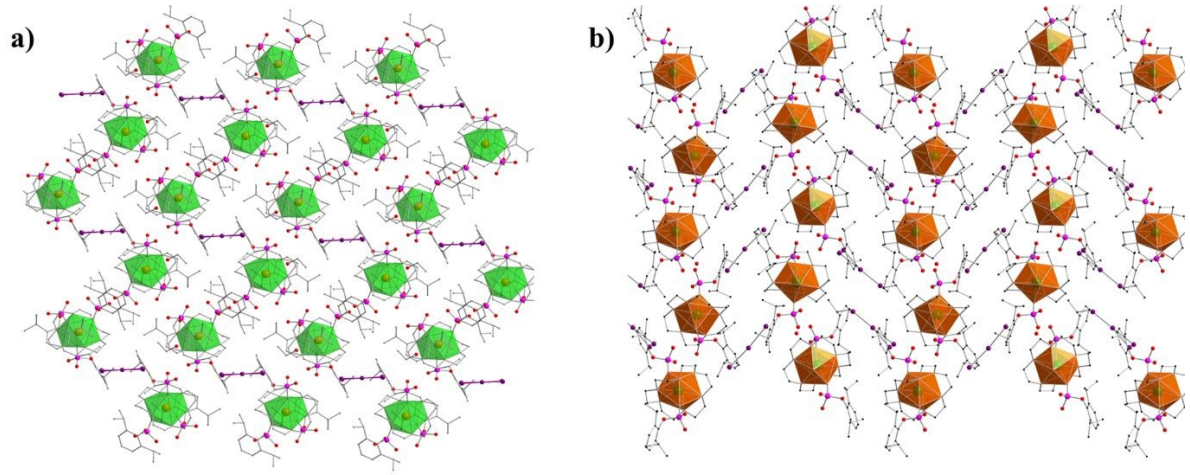

Figure 3. Lattice arrangement of (a) **2** and (b) **5** viewed along b-axis. H atoms are omitted for clarity, disordered I_3 ions with largest occupancy is shown here. Colour code: Pr, orange; P, pink; O, red; black, carbon and I, violet. Due to the bulkiness in the phenyl rings and lattice triiodide anions and solvent molecules, Ln(III) centres are separated by at least 9.83 Å (in **2**) and 10.84 Å (in **5**).

SHAPE analysis of 1-5. The coordination environments around the nine-coordinated Ln(III) ions have been analysed by continuous SHAPE measurements using SHAPE 2.1 software[69]. The continuous SHAPE

measurements reveal that the {LnO_9} cores in **1-5** has minimal deviation from the ideal *C*s symmetry, indicating a muffin shaped geometry around the Ln(III) ions in all the five complexes **1-5**. The muffin shaped polyhedra of **1** and **5** are shown in Figures 1c and 2d (also see ESI). The deviation from the perfect geometry in {LnO_9} core is listed in table S8.

Effect of lanthanide contraction: The difference in axial coordination in **1-3** (three phosphates) from **4**, **5** (two phosphates and one water molecule) is consistent with the lanthanide contraction. Due to the gradual decreasing ionic radii from Ce(III) to Eu(III), three sterically hindered phosphates are not able to find enough room for coordination to Ln(III) centres in **4** and **5**, instead, the third position is occupied by a sterically dwarf water molecule. To understand the effect of size of the Ln(III) ions, we have sanalysed the effect of lanthanide contraction on the average Ln-O bond lengths. It has been observed that the average Ln-O bond lengths decreases gradually from **1-5** with the same trend of decreasing ionic size. The decreasing Ln-O distance and the ionic radii due to lanthanide contraction is portrayed in Figure 4 and Table 3.

Table 3: Ln-O bond comparison in **1-5**.

Complex	Average Ln-O (axial) /Å	Average Ln-O (equatorial) /Å	Average Ln-O /Å	Ionic radii of Ln(III) /Å
1	2.383	2.654	2.564	10.10
2	2.362	2.622	2.535	9.90
3	2.351	2.608	2.522	9.83
4	2.324	2.559	2.481	9.58
5	2.292	2.560	2.471	94.7

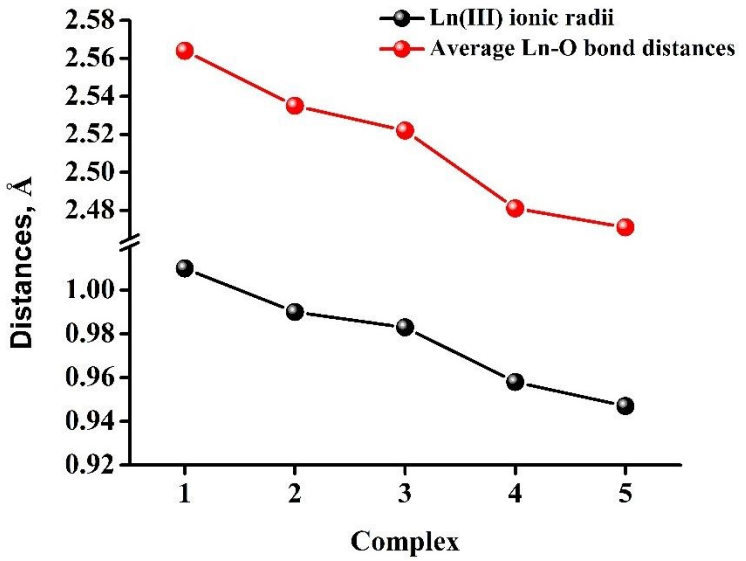

Figure 4. The plot of average Ln-O bond lengths in **1-5** (red) and ionic radii of different Ln(III) ions in octahedral symmetry (black). The variation in the average Ln-O bond lengths exactly follows the lanthanide contraction trend. The ionic radii of trivalent lanthanide ions are taken from Shannon-Prewitt ionic radius.[70]

***Power X-ray diffraction studies of 1-5*:** In order to confirm the phase purity of the compounds in bulk amount, powder X-Ray diffraction (PXRD) analysis were being carried out on the polycrystalline samples of **1-5**. The agreement of the experiemantal PXRD pattern with the simulated PXRD pattern obtained from the single crystal X-ray diffractometer analysis confirms the purity of these compounds in the bulk phase (Figure S11).

***Magnetic properties of* 1-4:** The static and dynamic properties of the crown-ether-based lanthanide organophosphates have been investigated with the help of direct current (dc) and alternating current (ac) magnetic

susceptibility measurements using an MPMS-XL SQUID magnetometer equipped with a 7.0 T magnet. All the magnetic measurements of **1**-**4** were carried out on the phase pure powered polycrystalline samples.

The temperature dependence of magnetisation is carried out in the temperature range of 2-300 K under an applied field of 1000 Oe. The $\chi_M T$ values obtained experimentally for **1-4** are 0.94 cm^3 K mol^{-1}, 1.45 cm^3 K mol^{-1}, 1.48 cm^3 K mol^{-1} and 0.48 cm^3Kmol^{-1}, respectively. These values are in good agreement with the calculated values for the respective isolated non-interacting lanthanide ions, except Sm(III), at 300 K [Ce(III) ion: ground state term: $^2F_{5/2}$, calculated $\chi_M T$ value: 0.81 cm^3 K mol^{-1}; Pr(III) ion: ground state term: $^3H_4$, calculated $\chi_M T$ value: 1.60 cm^3 K mol^{-1}; Nd(III) ion: ground state term: $^4I_{9/2}$, calculated $\chi_M T$ value: 1.64 cm^3 K mol^{-1}; Sm(III) ion: ground state term: $^6H_{5/2}$ and calculated χ_MT value: 0.09 cm^3 K mol^{-1}]. The temperature dependence of magnetisation is depicted in Figure S12. The room temperature χ_MT value for **4** is higher than the calculated $\chi_M T$ value for an isolated non-interacting Sm(III) ion (S = 5/2, L = 5, J = 5/2, g_j = 2/7). The ground-state multiplet (J = 5/2) of the free ion Sm(III) is separated from the first excited multiplet (J = 7/2) by only a small energy separation. In consequence, the susceptibilities observed are usually higher in the case of the samarium complex due to the admixture of states, as witnessed in some reported complexes of samarium(III).[71]

To investigate the existence of magnetic anisotropy, ac susceptibility measurements have been carried out on the polycrystalline samples of **1-4** in the presence of an oscillating field of 3.5 Oe within a frequency range of 0.1-1500 Hz. None of the compounds shows frequency-dependent out-of-phase ac susceptibility signals (χ'') in the absence of any static magnetic field. This indicates that strong quantum tunnelling of magnetisation (QTM) is operative. As QTM can be quenched or partially suppressed by the application of an external magnetic field, the ac measurements were performed in the presence of the applied field. The field required to quench the QTM varies from molecule to molecule. At a specific external field, called an optimum field, QTM is suppressed to the greatest extent. The ac susceptibility measurements were carried out in the presence of various external fields in the range of 50-4000 Oe at 1.8K to determine the optimum magnetic field. Non-zero frequency dependent out-of-phase ac susceptibility signals (χ'') were observed for **1** and **3**. Still, there was no out-of-phase signals in the case of **2** and **4**, indicating that **1** and **3** behave as field-induced single-ion magnets. At the same time, **2** and **4** do not possess any such behaviour even on the application of a high dc magnetic field**.**

In the case of **1**, a small dc field of 350 Oe is enough to quench the undesired tunnelling to the greatest extent. Thus, all the ac susceptibility measurements have been carried out in the presence of this optimum dc magnetic field. Under the optimum magnetic field, there exists frequency dependence of out-of-phase magnetic susceptibility (χ'') signals in the temperature range of 1.8 K-3.6 K. The frequency dependent in-phase (χ') and out-of-phase susceptibility (χ'') components are shown in Figure 5a. There are two distinct relaxation pathways observed corresponding to the high-frequency peaks (fast relaxation, FR) and low-frequency peaks (slow relaxation, SR).[72] The two semicircular shaped Cole-Cole plot (χ' vs χ'') of **1** also confirms the existence of two relaxation processes (Figure 5c). Thus the plot is well-fitted to a modified Debye model, by considering two relaxation pathways, indicating the presence of a narrow distribution of relaxation time ($0.11<\alpha_1<0.17$ and $0.18<\alpha_2<0.27$) (table S9). The temperature dependence of relaxation time (τ) associated with **1** has been estimated by plotting $1/\tau$ vs 1/T (5e, 5f). The nonlinearity of the $1/\tau$ vs 1/T plot indicates the existence of more than one relaxation process in the relaxation dynamics of **1**. The dependency of relaxation time on temperature is different for different types of relaxation processes, except quantum tunnelling of magnetisation (QTM), which is not dependent on temperature. This can be summarised as follows:

$$1/\tau = 1/\tau_{QTM} + AT + CT^n + \tau_o^{-1} \exp(-U_{eff}/k_B T) \quad \text{..... Equation-1}$$

Where the first term on the right-hand side of equation-1 denotes the relaxation of magnetisation through QTM, the second and third terms represent the relaxation via direct and Raman processes respectively, and the last term corresponds to the thermally-assisted Orbach relaxation pathway.

The high temperature region of $1/\tau$ vs T plot is linearly fitted well using the Arrhenius equation, $\tau^{-1} = \tau_o^{-1} \exp(-U_{eff}/k_B T)$, estimating U_{eff} = 16.4(9) K, $\tau_0 = 6(1) \times 10^{-5}$ s for fast relaxation (FR) and U_{eff} = 16.3(2) K, $\tau_0 = 2(1) \times 10^{-6}$ s for slow relaxation (SR). The overall $1/\tau$ vs T plot can be best fitted by considering Orbach and QTM pathways (τ_{QTM} = 0.079 s in FR and 0.0025 s in SR). Even if the barrier heights for both the FR and SR are same,

View Article Online
DOI: 10.1039/D3DT01206A

there are two distinct relaxation processes (figure 5a and 5c). This is likely due to two structurally similar Ce(III) monomers possibly having different extents of dominance of QTM and Orbach processes in the overall relaxation dynamics of **1**. These barrier heights associated with **1** are comparable with the previously reported Ce(III) based single-ion magnets (Table 1).[34, 49-52, 73-75] The fitting of the nonlinear plot of $1/\tau$ vs T is depicted in Figure 5e-5f.

Similar to **1**, χ'' signals were absent in the case of **3** in the absence of any bias magnetic field. Thus, the optimum field is determined by collecting χ'' signals at 1.8 K in the frequency range of 0.1-1500 Hz from 0 to 4000 Oe (figure S14). The QTM functioned on **3** is suppressed/quenched to the greatest extent in the presence of the optimum dc field, *viz.* 1500 Oe. Under this optimum field, frequency and temperature dependence χ'' signals were observed up to a temperature range of 1.8-2.6 K. Frequency-dependent in-phase (χ') and out-of-phase susceptibility (χ'') components for **3** are depicted in Figure 5b which clearly show a single maximum over the whole frequency range which shift towards higher frequency on increasing temperature. The Cole-Cole plot of **3** confirms that the single relaxation process is operative throughout the relaxation, unlike **1**. The Cole-Cole plot is fitted with a generalised Debye equation (Figure 5d). The fitting shows a very narrow distribution of relaxation time with α range of 0.08 to 0.11 (Table S10). The temperature dependence of relaxation time (τ) for **3** can be obtained by plotting $1/\tau$ vs T. The linear plot of $1/\tau$ vs T can be well fitted by the Orbach process, considering the Arrhenius equation, with $U_{\text{eff}} = 6.0$ K and $\tau_o = 1.0 \times 10^{-5}$ s. However, at the low temperature range (up to 3K), the Raman as well as the QTM are operative over the Orbach process. Attempts to fit the plot considering different combinations of relaxation processes other than Orbach were not successful. This plot can be best fitted by considering only Raman process with the parameters $C = 10^{2.7(8)}$ s^{-1} K^{-n} and n=3(2). Thus, the slow relaxation of magnetisation dynamics in **3** is dominated by the Raman process.

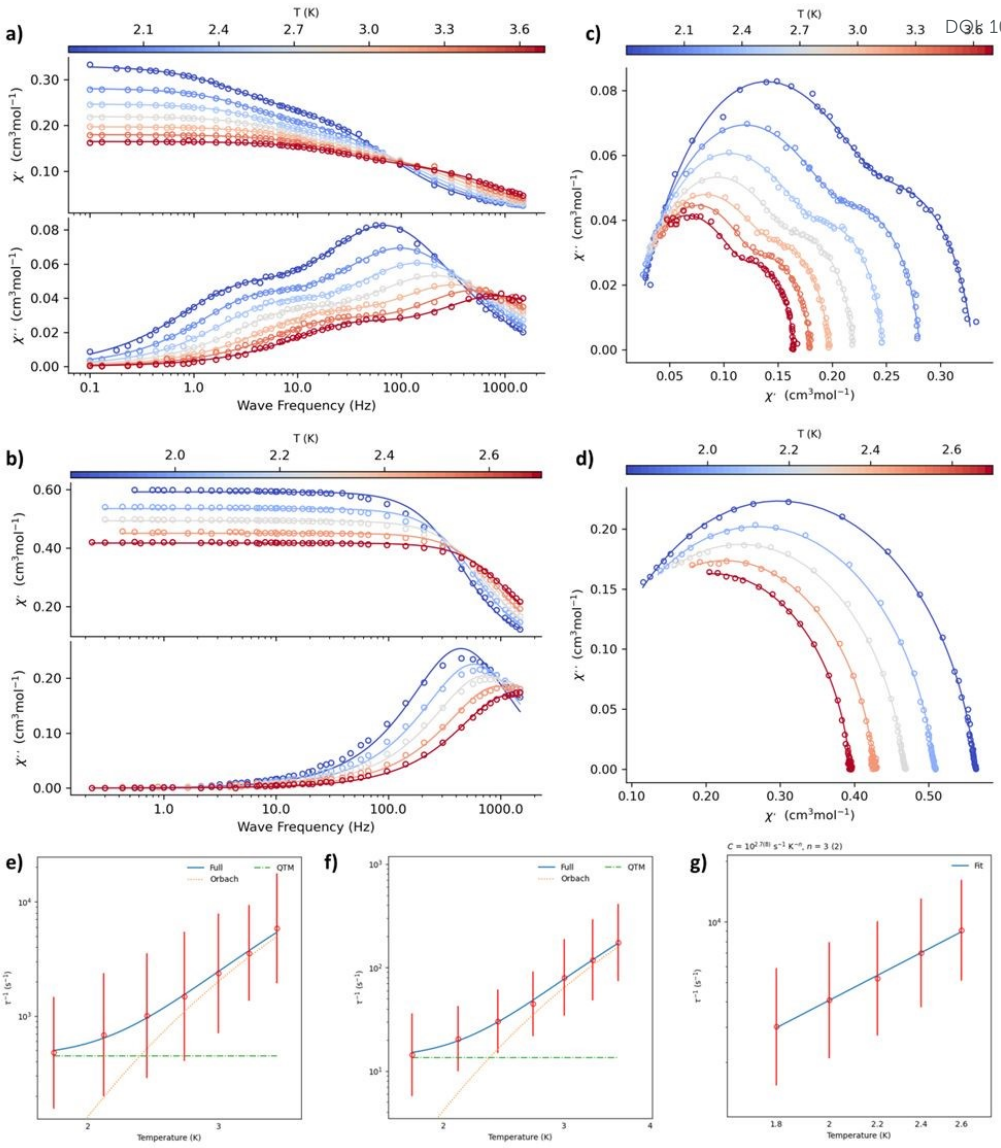

Figure 5: Frequency-dependent in-phase and out-of-phase susceptibility signals of (a) **1** and (b) **3** at the indicated temperature range in the presence of an external magnetic field (350 Oe for **1** and 1500 Oe for **3**). The cole-cole plot of (c) **1** and (d) **3**. The plot of $1/\tau$ vs T for (e-f) **1** and (g) **3**. The plots for **1** are well fitted by considering Orbach (dotted red) and QTM (dotted green) (5e corresponds to SR and 5f corresponds to FR), while that of **3** are well fitted by considering Raman process.

The ac susceptibility measurements on **2** and **4** were also carried out to find whether these molecules can possess any slow relaxation of magnetisation behaviour. However, there is no significant frequency dependence in phase and out-of-phase magnetic susceptibility signals observed even in the presence of an external magnetic field. This suggests that **2** and **4** do not behave as single-ion magnets**.**

Theoretical calculations. To get further insight into the magnetisation relaxation, the ab initio CASSCF/RASSI-SO/SINGLE_ANISO calculations were performed on complexes **1** and **3** using MOLCAS 8.2 program package. The Ce(III) and Nd(III) ions possess $4f^1$ and $4f^3$ electron configurations, resulting in the $^2F_{5/2}$ and $^4I_{9/2}$ ground states, respectively. The ab initio calculations unveil axial anisotropy in both complexes with relatively large g_z values (Table 4-5). We have estimated the crystal field parameters in both complexes using Stevens Hamiltonian, $\hat{H}_{CF} = \sum_{k=2,4,6} \sum_{q=-k}^{q=+k} B_k^q \tilde{O}_k^q$, where B_k^q is the crystal field parameter (CFP) and $\tilde{O}_k^q$ is the Stevens operator. The probability of QTM becomes higher when non-axial terms (k = 2, 4, 6 and q ≠ 0) are larger or comparable to the axial terms (k = 2, 4, 6 and q = 0). Here, the negative B_2^0 values indicate the significant axiality in both complexes (Table 4). The computed g tensor (g_x = 0.553, g_y = 0.784 and g_z = 3.670 for **1** and g_x = 0.590, g_y = 1.041 and g_z = 5.390 for **3**, see Table 4-5) reveals significant transverse anisotropy in the ground KD which is also reflected in the calculated non-negligible QTM values of ca 0.20 μ_B (see Figure 6a-6d). The ground state of complexes **1** and **3** are found to possess a dominant contribution from m_J = |±5/2> and m_J = |±9/2>, respectively, where non-negligible mixing among other states explains the field-induced SIM behaviour of both complexes. The orientation of the computed g_{zz} axis is shown in Figure 6. Basically, it is oriented in such a way that it avoids the oblate 4f electron density in the ground state and 4f electron density lies along the longest metal-ligand bond. A very large QTM computed reveals that these molecules are unlikely to exhibit SIM behaviour at zero-field, as observed in the experiments. However, if a very large magnetic field is applied, this may partially quench the QTM at the ground state allowing relaxation via the first excited state. As demonstrated in the experiments, the optimum field for **1** and **3** are 350 Oe and 1500 Oe, respectively. We have then extended the mechanism to the first excited state, assuming complete quenching of the ground state QTM, though this is expected to overestimate the theoretical barrier height.

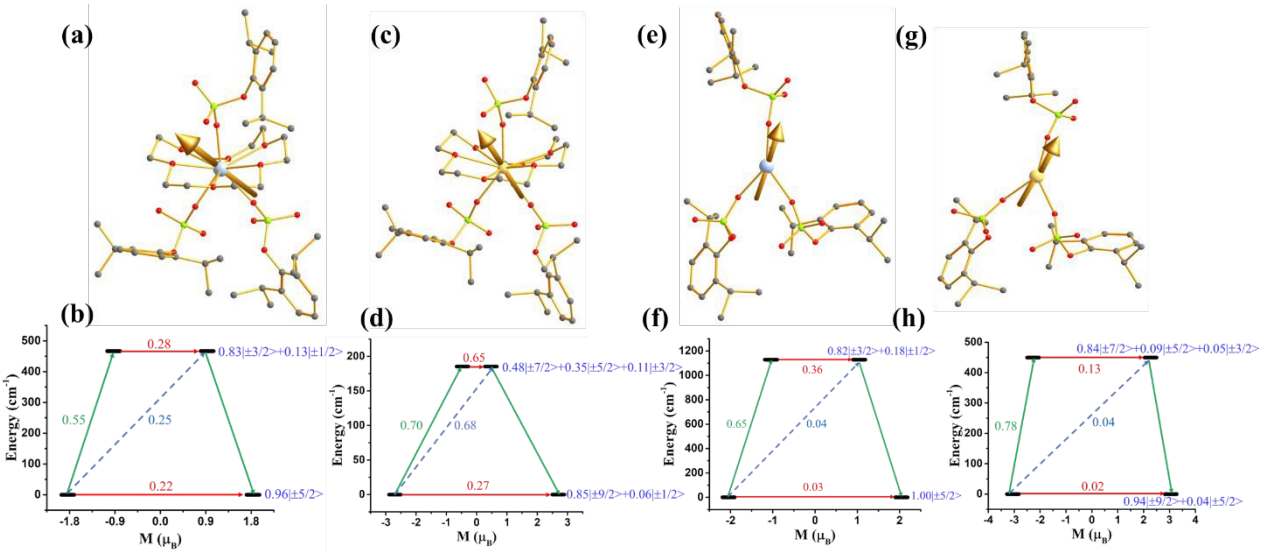

Figure 6: The computed g_{zz} axis of the ground state of complex (a) **1** (c) **3** (e) **1a**, (g) **3a**. Colour code: Ce-blue white, Nd-yellow, P-green, O-red, C-grey. Hydrogens are omitted for clarity. The mechanism of magnetisation relaxation of (c) **1** (d) **3**. Here, the red arrows denote the QTM via the ground state and TA-QTM via the first excited state. The blue arrow denotes the Orbach process, and the green arrow signifies the most probable pathway of magnetisation relaxation. The blue characters represent the m_J composition of a KD.

The computed three KDs (belonging to $^2F_{5/2}$) for **1** are found to span up to 978.8 cm^{-1}, while the five KDs (belonging to $^4I_{9/2}$) for **3** span up to 480.0 cm^{-1}. The first excited KDs show significant mixing among m_J states (m_J = |±3/2> and |±7/2> is dominant for **1** and **3** respectively) which leads to the very large transverse anisotropy (g_x = 0.134, g_y = 0.947 and g_z = 2.523 for **1** and g_x = 3.180, g_y = 1.906 and g_z = 0.357 for **3**, see Table 4-5). This promotes significant TA-QTM (thermally assisted QTM) for magnetisation relaxation. On the other hand, the g_{zz} axis of the first excited KDs strongly deviates from the ground KDs, reinforcing the magnetisation relaxation via the first excited KDs (Table 4-5). This results in the U_{cal} value of 467.0 and 185.3 cm^{-1} for complexes **1** and **3,** respectively. The computed U_{cal} values are significantly overestimated compared to the experimental U_{eff} values, as expected. The larger U_{cal} value of **1** compared to **3** can be explained by the larger value of B_2^0 CFP in the former compared to

the latter (Table S11). This is also correlated with the computed Loprop charges, where the charges in the crown ether are lower in **1** compared to **3**, resulting in a stronger stabilisation of the oblate electron density in the former (see Table S12).

To determine the role of equatorial crown ether in the magnetisation relaxation dynamics, we have removed 18-crown-6 from complexes **1** and **3**, resulting in models **1a** and **3a,** respectively (Figures 6e and 6h). The ab initio calculations on model **1a** and **3a** reveal quenching of QTM in the ground KDs, which is reflected in the negligible transverse anisotropy (g_x = 0.063, g_y = 0.134, g_z = 4.089 for **1a** and g_x = 0.049, g_y = 0.062, g_z = 6.096 for **3a**, see Figures 6f and 6h, Tables S13-14). This is also reflected in large B_2^0 CF parameter and almost pure m_J ground state (Tables S11 and S13-14). Furthermore, the computed KDs are found to span 2179.1 and 830.3 cm^{-1} in **1a** and **3a,** respectively, two times larger than **1** and **3** (Figures 6f and 6h). The magnetisation relaxation occurs via second excited KDs due to the significant TA-QTM and large deviation of the g_z axis with the ground state. This results in the U_{cal} value of 1128.2 and 449.6 cm^{-1} for **1a** and **3a,** respectively. A large increase in the U_{cal} value in the model complexes can be ascribed to a large equatorial ligand field from six oxygen donor atoms of the crown ligand and also its non-planarity. Therefore to increase the blocking barrier, the number of donor atoms in the crown ligand can be decreased. Removing one of the organophosphates at the axial position by employing a bulkier phosphate would also significantly strengthen the axiality and improve the SIM characteristics.

Table 4. The CASSCF/RASSI-SO/SINGLE_ANISO calculated g tensor, m_J composition and g_{zz} angles of three ground state KDs of **1**.

Energy (cm^{-1})	g_x	g_y	g_z	m_J composition	Angle between g_{zz} of higher KDs with KD1 (°)
0.0	0.553	0.784	3.670	0.96|±5/2>	
467.0	0.134	0.947	2.523	0.83|±3/2>+0.13|±1/2>	46.5
978.8	0.589	1.642	3.261	0.85|±1/2>+0.13|±3/2>	76.7

Table 5. The CASSCF/RASSI-SO/SINGLE_ANISO calculated g tensor, m_J composition and g_{zz} angles of three ground state KDs of **3**.

Energy (cm^{-1})	g_x	g_y	g_z	m_J composition	Angle between g_{zz} of higher KDs with KD1 (°)
0.0	0.590	1.041	5.390	0.85|±9/2>+0.06|±1/2>	
185.3	3.180	1.906	0.357	0.48|±7/2>+0.35|±5/2>+0.11|±3/2>	27.5
256.1	0.570	1.704	4.250	0.42|±3/2>+0.39|±5/2>+0.06|±7/2>	111.3
366.0	0.029	0.889	4.019	0.54|±1/2>+0.24|±3/2>+0.12|±7/2>	90.2
480.0	0.343	0.866	4.432	0.30|±7/2>+0.28|±1/2>+0.20|±5/2>+0.18|±3/2>	94.6

Conclusions

Placing an equatorial ligand-field through hexadentate 18-crown-6 and facilitating further coordination by a bulky phosphate ($dippH_2$) or water ligand in the axial positions, five new mononuclear early Ln(III) organophosphate have been synthesised and characterised. Single-crystal X-ray diffraction studies reveal that Ln(III) centres in all the five complexes are in muffin-shaped coordination sphere, where the equatorial plane is occupied by 18-crown-6 molecule while three phosphates are present in the axial positions in **1-3** or two phosphates along with one water are present in the axial positions in **4** and **5.** Such structural modifications are attributable to the lanthanide contraction. Both dc and ac susceptibility measurements carried out on **1-4** reveal that **1** and **3** exhibit slow relaxation of magnetisation in the presence of applied magnetic field. The relaxation dynamics associated with the slow relaxation of magnetisation of **1** and **3** have been investigated in detail, unveiling a rare pair of field-induced Ce and Nd SIMs with a performance similar to a handful of examples reported so far. The CASSCF calculations reveal that the ligand stabilises the highest m_J as the ground state for both the Ce and Nd complexes, but the transverse anisotropy is significant that facilitates strong ground state QTM effects. Efforts are underway in our laboratory to improve the SIM characteristics further by designing bulkier organophosphate ligands.

View Article Online
DOI: 10.1039/D3DT01206A

Acknowledgement

We thank SERB (SB/SJF/2019-20/12; SPR/2019/001145; CRG/2022/001697) for funding. SD thanks IITB for IPDF fellowship.

References

1. Sessoli, R.; Gatteschi, D.; Caneschi, A.; Novak, M., Magnetic bistability in a metal-ion cluster. *Nature* **1993,** *365* (6442), 141-143.
2. Donati, F.; Rusponi, S.; Stepanow, S.; Wäckerlin, C.; Singha, A.; Persichetti, L.; Baltic, R.; Diller, K.; Patthey, F.; Fernandes, E., Magnetic remanence in single atoms. *Science* **2016,** *352* (6283), 318-321.
3. Natterer, F. D.; Yang, K.; Paul, W.; Willke, P.; Choi, T.; Greber, T.; Heinrich, A. J.; Lutz, C. P., Reading and writing single-atom magnets. *Nature* **2017,** *543* (7644), 226-228.
4. Ishikawa, N.; Sugita, M.; Ishikawa, T.; Koshihara, S.-y.; Kaizu, Y., Lanthanide double-decker complexes functioning as magnets at the single-molecular level. *J. Am. Chem. Soc.* **2003,** *125* (29), 8694-8695.
5. Gupta, S. K.; Murugavel, R., Enriching lanthanide single-ion magnetism through symmetry and axiality. *ChemComm* **2018,** *54* (30), 3685-3696.
6. Woodruff, D. N.; Winpenny, R. E.; Layfield, R. A., Lanthanide single-molecule magnets. *Chem. Rev.* **2013,** *113* (7), 5110-5148.
7. Guo, F.-S.; Day, B. M.; Chen, Y.-C.; Tong, M.-L.; Mansikkamäki, A.; Layfield, R. A., Magnetic hysteresis up to 80 kelvin in a dysprosium metallocene single-molecule magnet. *Science* **2018,** *362* (6421), 1400-1403.
8. Goodwin, C. A.; Ortu, F.; Reta, D.; Chilton, N. F.; Mills, D. P., Molecular magnetic hysteresis at 60 kelvin in dysprosocenium. *Nature* **2017,** *548* (7668), 439-442.
9. Evans, P.; Reta, D.; Whitehead, G. F.; Chilton, N. F.; Mills, D. P., Bis-monophospholyl dysprosium cation showing magnetic hysteresis at 48 K. *J. Am. Chem. Soc.* **2019,** *141* (50), 19935-19940.
10. Stamp, P. C.; Gaita-Arino, A., Spin-based quantum computers made by chemistry: hows and whys. *J. Mater. Chem.* **2009,** *19* (12), 1718-1730.
11. Leuenberger, M. N.; Loss, D., Quantum computing in molecular magnets. *Nature* **2001,** *410* (6830), 789-793.
12. Aromí, G.; Aguila, D.; Gamez, P.; Luis, F.; Roubeau, O., Design of magnetic coordination complexes for quantum computing. *Chem. Soc. Rev.* **2012,** *41* (2), 537-546.
13. Affronte, M., Molecular nanomagnets for information technologies. *Journal of Materials Chemistry* **2009,** *19* (12), 1731-1737.
14. Urdampilleta, M.; Klyatskaya, S.; Cleuziou, J.-P.; Ruben, M.; Wernsdorfer, W., Supramolecular spin valves. *Nat. Mater.* **2011,** *10* (7), 502-506.
15. Rocha, A. R.; Garcia-Suarez, V. M.; Bailey, S. W.; Lambert, C. J.; Ferrer, J.; Sanvito, S., Towards molecular spintronics. *Nat. Mater.* **2005,** *4* (4), 335-339.
16. Vincent, R.; Klyatskaya, S.; Ruben, M.; Wernsdorfer, W.; Balestro, F., Electronic read-out of a single nuclear spin using a molecular spin transistor. *Nature* **2012,** *488* (7411), 357-360.
17. Mannini, M.; Pineider, F.; Sainctavit, P.; Danieli, C.; Otero, E.; Sciancalepore, C.; Talarico, A. M.; Arrio, M.-A.; Cornia, A.; Gatteschi, D.; Sessoli, R., Magnetic memory of a single-molecule quantum magnet wired to a gold surface. *Nat. Mater.* **2009,** *8* (3), 194-197.
18. Winpenny, R. E., Quantum information processing using molecular nanomagnets as qubits. *Angew. Chem. Int. Ed.* **2008,** *47* (42), 7992-7994.
19. McAdams, S. G.; Ariciu, A.-M.; Kostopoulos, A. K.; Walsh, J. P.; Tuna, F., Molecular single-ion magnets based on lanthanides and actinides: Design considerations and new advances in the context of quantum technologies. *Coord. Chem. Rev.* **2017,** *346*, 216-239.
20. Harriman, K. L.; Errulat, D.; Murugesu, M., Magnetic axiality: Design principles from molecules to materials. *Trends Chem.* **2019,** *1* (4), 425-439.
21. Dey, M.; Gogoi, N., Geometry-Mediated Enhancement of Single-Ion Anisotropy: A Route to Single-Molecule Magnets with a High Blocking Temperature. *Angew. Chem. Int. Ed.* **2013,** *52* (49), 12780-12782.
22. Rechkemmer, Y.; Breitgoff, F. D.; Van Der Meer, M.; Atanasov, M.; Hakl, M.; Orlita, M.; Neugebauer, P.; Neese, F.; Sarkar, B.; Van Slageren, J., A four-coordinate cobalt (II) single-ion magnet with coercivity and a very high energy barrier. *Nat. Commun.* **2016,** *7* (10467), 10467.
23. Zhu, Z.; Zhao, C.; Feng, T.; Liu, X.; Ying, X.; Li, X.-L.; Zhang, Y.-Q.; Tang, J., Air-stable chiral single-molecule magnets with record anisotropy barrier exceeding 1800 K. *J. Am. Chem. Soc.* **2021,** *143* (27), 10077-10082.
24. Zhu, Z.; Tang, J., Metal–metal bond in lanthanide single-molecule magnets. *Chem. Soc. Rev.* **2022**.

25. Borah, A.; Murugavel, R., Magnetic relaxation in single-ion magnets formed by less-studied lanthanide ions Ce (III), Nd (III), Gd (III), Ho (III), Tm (II/III) and Yb (III). *Coord. Chem. Rev.* **2022,** *453*, 214288.
26. Zhu, Z.; Tang, J., Lanthanide single-molecule magnets with high anisotropy barrier: where to from here? *National Science Review* **2022,** *9* (12), nwac194.
27. Borah, A.; Dey, S.; Gupta, S. K.; Walawalkar, M. G.; Rajaraman, G.; Murugavel, R., Enhancing the barrier height for Yb (iii) single-ion magnets by modulating axial ligand fields. *ChemComm* **2020,** *56* (79), 11879-11882.
28. Deheri, P. K.; Swaminathan, V.; Bhame, S. D.; Liu, Z.; Ramanujan, R. V., Sol− gel based chemical synthesis of Nd2Fe14B hard magnetic nanoparticles. *Chem. Mater.* **2010,** *22* (24), 6509-6517.
29. Pathak, A. K.; Khan, M.; Gschneidner Jr, K. A.; McCallum, R. W.; Zhou, L.; Sun, K.; Dennis, K. W.; Zhou, C.; Pinkerton, F. E.; Kramer, M. J., Cerium: an unlikely replacement of dysprosium in high performance Nd–Fe–B permanent magnets. *Adv. Mater.* **2015,** *27* (16), 2663-2667.
30. Rinehart, J. D.; Long, J. R., Exploiting single-ion anisotropy in the design of f-element single-molecule magnets. *Chem. Sci.* **2011,** *2* (11), 2078-2085.
31. Mautner, F. A.; Bierbaumer, F.; Fischer, R. C.; Tubau, A. n.; Speed, S.; Ruiz, E.; Massoud, S. S.; Vicente, R.; Gómez-Coca, S., Insights into the Spin Dynamics of Mononuclear Cerium (III) Single-Molecule Magnets. *Inorganic Chemistry* **2022**.
32. Canaj, A. B.; Dey, S.; Martí, E. R.; Wilson, C.; Rajaraman, G.; Murrie, M., Insight into D6h Symmetry: Targeting Strong Axiality in Stable Dysprosium (III) Hexagonal Bipyramidal Single-Ion Magnets. *Angew. Chem. Int. Ed.* **2019,** *58* (40), 14146-14151.
33. Li, Z. H.; Zhai, Y. Q.; Chen, W. P.; Ding, Y. S.; Zheng, Y. Z., Air-Stable Hexagonal Bipyramidal Dysprosium (III) Single-Ion Magnets with Nearly Perfect D6h Local Symmetry. *Chem. Eur. J.* **2019,** *25* (71), 16219-16224.
34. Wada, H.; Ooka, S.; Yamamura, T.; Kajiwara, T., Light lanthanide complexes with crown ether and its Aza derivative which show slow magnetic relaxation behaviors. *Inorg. Chem.* **2017,** *56* (1), 147-155.
35. Ding, Y.-S.; Han, T.; Hu, Y.-Q.; Xu, M.; Yang, S.; Zheng, Y.-Z., Syntheses, structures and magnetic properties of a series of mono-and di-nuclear dysprosium (iii)-crown-ether complexes: effects of a weak ligand-field and flexible cyclic coordination modes. *Inorganic Chemistry Frontiers* **2016,** *3* (6), 798-807.
36. Gavey, E. L.; Al Hareri, M.; Regier, J.; Carlos, L. D.; Ferreira, R. A.; Razavi, F. S.; Rawson, J. M.; Pilkington, M., Placing a crown on Dy III–a dual property Ln III crown ether complex displaying optical properties and SMM behaviour. *J. Mater. Chem. C* **2015,** *3* (29), 7738-7747.
37. Gao, F.; Yang, F.-L.; Feng, X.; Xu, H.; Sun, W.; Liu, H.; Li, X.-L., Half-sandwich lanthanide crown ether complexes with the slow relaxation of magnetization and photoluminescence behaviors. *Dalton Trans.* **2017,** *46* (4), 1317-1323.
38. Bar, A. K.; Kalita, P.; Singh, M. K.; Rajaraman, G.; Chandrasekhar, V., Low-coordinate mononuclear lanthanide complexes as molecular nanomagnets. *Coord. Chem. Rev.* **2018,** *367*, 163-216.
39. Gupta, S. K.; Langley, S. K.; Sharma, K.; Murray, K. S.; Murugavel, R., Pentanuclear lanthanide mono-organophosphates: synthesis, structure, and magnetism. *Inorg. Chem.* **2017,** *56* (7), 3946-3960.
40. Gupta, S. K.; Bhat, G. A.; Murugavel, R., Lanthanide organophosphate spiro polymers: synthesis, structure, and magnetocaloric effect in the gadolinium polymer. *Inorg. Chem.* **2017,** *56* (15), 9071-9083.
41. Gupta, S. K.; Dar, A. A.; Rajeshkumar, T.; Kuppuswamy, S.; Langley, S. K.; Murray, K. S.; Rajaraman, G.; Murugavel, R., Discrete {Gd III 4 M}(M= Gd III or Co II) pentanuclear complexes: a new class of metal-organophosphate molecular coolers. *Dalton Trans.* **2015,** *44* (13), 5961-5965.
42. Sharma, K.; Gupta, S. K.; Borah, A.; Murugavel, R., Hitherto unknown eight-connected frameworks formed from A 4 B 4 O 12 metal organophosphate heterocubanes. *ChemComm* **2019,** *55* (55), 7994-7997.
43. Li, Q.-W.; Wan, R.-C.; Chen, Y.-C.; Liu, J.-L.; Wang, L.-F.; Jia, J.-H.; Chilton, N. F.; Tong, M.-L., Unprecedented hexagonal bipyramidal single-ion magnets based on metallacrowns. *ChemComm* **2016,** *52* (91), 13365-13368.
44. Cai, X.; Cheng, Z.; Wu, Y.; Jing, R.; Tian, S.-Q.; Chen, L.; Li, Z.-Y.; Zhang, Y.-Q.; Cui, H.-H.; Yuan, A., Tuning the Equatorial Negative Charge in Hexagonal Bipyramidal Dysprosium (III) Single-Ion Magnets to Improve the Magnetic Behavior. *Inorg. Chem.* **2022,** *61* (8), 3664-3673.
45. Zhao, W.; Cui, H.; Chen, X.-Y.; Yi, G.; Chen, L.; Yuan, A.; Luo, C.-L., An eight-coordinate ytterbium complex with a hexagonal bipyramid geometry exhibiting field-induced single-ion magnet behaviour. *Dalton Trans.* **2019,** *48* (17), 5621-5626.
46. Li, J.; Gómez-Coca, S.; Dolinar, B. S.; Yang, L.; Yu, F.; Kong, M.; Zhang, Y.-Q.; Song, Y.; Dunbar, K. R., Hexagonal bipyramidal Dy (III) complexes as a structural archetype for single-molecule magnets. *Inorg. Chem.* **2019,** *58* (4), 2610-2617.
47. Ding, Y.-S.; Blackmore, W. J.; Zhai, Y.-Q.; Giansiracusa, M. J.; Reta, D.; Vitorica-Yrezabal, I.; Winpenny, R. E.; Chilton, N. F.; Zheng, Y.-Z., Studies of the Temperature Dependence of the Structure and

Magnetism of a Hexagonal-Bipyramidal Dysprosium (III) Single-Molecule Magnet. *Inorg. Chem.* **2021,** *60* (1), 227-235.
48. Zhao, C.; Zhu, Z.; Li, X.-L.; Tang, J., Air-stable chiral mono-and dinuclear dysprosium single-molecule magnets: steric hindrance of hexaazamacrocycles. *Inorg. Chem. Front.* **2022,** *9* (16), 4049-4055.
49. Le Roy, J. J.; Korobkov, I.; Kim, J. E.; Schelter, E. J.; Murugesu, M., Structural and magnetic conformation of a cerocene [Ce (COT″) 2]− exhibiting a uniconfigurational f 1 ground state and slow-magnetic relaxation. *Dalton Trans.* **2014,** *43* (7), 2737-2740.
50. Upadhyay, A.; Vignesh, K. R.; Das, C.; Singh, S. K.; Rajaraman, G.; Shanmugam, M., Influence of the ligand field on the slow relaxation of magnetization of unsymmetrical monomeric lanthanide complexes: synthesis and theoretical studies. *Inorg. Chem.* **2017,** *56* (22), 14260-14276.
51. Xu, M.-X.; Meng, Y.-S.; Xiong, J.; Wang, B.-W.; Jiang, S.-D.; Gao, S., Magnetic anisotropy investigation on light lanthanide complexes. *Dalton Trans.* **2018,** *47* (6), 1966-1971.
52. Gupta, S. K.; Shanmugan, S.; Rajeshkumar, T.; Borah, A.; Damjanović, M.; Schulze, M.; Wernsdorfer, W.; Rajaraman, G.; Murugavel, R., A single-ion single-electron cerrous magnet. *Dalton Trans.* **2019,** *48* (42), 15928-15935.
53. Mautner, F. A.; Bierbaumer, F.; Fischer, R. C.; Tubau, À.; Speed, S.; Ruiz, E.; Massoud, S. S.; Vicente, R.; Gómez-Coca, S., Insights into the Spin Dynamics of Mononuclear Cerium (III) Single-Molecule Magnets. *Inorg. Chem.* **2022,** *61* (29), 11124-11136.
54. Leng, J.-D.; Hua, Q.-Y.; Liu, W.-T.; Tao, Z.-X.; Tan, N.-W.; Wang, Y.-F.; Lin, W.-Q., Slow magnetic relaxation of mononuclear complexes based on uncommon Kramers lanthanide ions Ce III, Sm III and Yb III. *Dalton Trans.* **2022,** *51* (33), 12661-12669.
55. Rinehart, J. D.; Long, J. R., Slow magnetic relaxation in homoleptic trispyrazolylborate complexes of neodymium (III) and uranium (III). *Dalton Trans.* **2012,** *41* (44), 13572-13574.
56. Le Roy, J. J.; Gorelsky, S. I.; Korobkov, I.; Murugesu, M., Slow magnetic relaxation in uranium (III) and neodymium (III) cyclooctatetraenyl complexes. *Organometallics* **2015,** *34* (8), 1415-1418.
57. Wada, H.; Ooka, S.; Iwasawa, D.; Hasegawa, M.; Kajiwara, T., Slow magnetic relaxation of lanthanide (III) complexes with a helical ligand. *Magnetochemistry* **2016,** *2* (4), 43.
58. Gupta, S. K.; Rajeshkumar, T.; Rajaraman, G.; Murugavel, R., An unprecedented zero field neodymium (III) single-ion magnet based on a phosphonic diamide. *ChemComm* **2016,** *52* (44), 7168-7171.
59. Chen, Y.-C.; Huang, X.-S.; Liu, J.-L.; Tong, M.-L., Magnetic Dynamics of a Neodymium (III) Single-Ion Magnet. *Inorg. Chem.* **2018,** *57* (18), 11782-11787.
60. Demir, S.; Meihaus, K. R.; Long, J. R., Slow magnetic relaxation in a neodymium metallocene tetraphenylborate complex. *J. Organomet. Chem.* **2018,** *857*, 164-169.
61. Kumar, K.; Abe, D.; Komori-Orisaku, K.; Stefańczyk, O.; Nakabayashi, K.; Shakirova, J. R.; Tunik, S. P.; Ohkoshi, S.-i., Neodymium β-diketonate showing slow magnetic relaxation and acting as a ratiometric thermometer based on near-infrared emission. *RSC advances* **2019,** *9* (41), 23444-23449.
62. Li, J.; Yin, L.; Xiong, S.-J.; Wu, X.-L.; Yu, F.; Ouyang, Z.-W.; Xia, Z.-C.; Zhang, Y.-Q.; van Tol, J.; Song, Y.; Wang, Z., Controlling Electron Spin Decoherence in Nd-based Complexes via Symmetry Selection. *Iscience* **2020,** *23* (3), 100926.
63. Armarego, W. L. F., *Purification of laboratory chemicals*. Butterworth-Heinemann: 2017; Vol. 8.
64. Kosolapoff, G. M.; Arpke, C. K.; Lamb, R. W.; Reich, H., Structural effects in reactions of organophosphorus compounds. I. Reactions of phosphorus oxychloride with hindered phenols. *J. Chem. Soc. C* **1968**, 815-818.
65. Dolomanov, O. V.; Bourhis, L. J.; Gildea, R. J.; Howard, J. A.; Puschmann, H., OLEX2: a complete structure solution, refinement and analysis program. *J. Appl. Crystallogr.* **2009,** *42* (2), 339-341.
66. Sheldrick, G. M., SHELXT: Integrating space group determination and structure solution. *Acta Crystallogr., Sect. A: Found. Adv* **2014,** *70*, C1437.
67. Sheldrick, G. M., Crystal structure refinement with SHELXL. *Acta Crystallogr. C Struct. Chem.* **2015,** *71* (1), 3-8.
68. Reta, D.; Chilton, N. F., Uncertainty estimates for magnetic relaxation times and magnetic relaxation parameters. *Phys. Chem. Chem. Phys.* **2019,** *21* (42), 23567-23575.
69. Llunell, M.; Casanova, D.; Cirera, J.; Alemany, P.; Alvarez, S., SHAPE, version 2.1. *Universitat de Barcelona, Barcelona, Spain* **2013,** *2103*.
70. Shannon, R. D., Revised effective ionic radii and systematic studies of interatomic distances in halides and chalcogenides. *Acta Crystallogr A.* **1976,** *32* (5), 751-767.
71. Chakraborty, J.; Ray, A.; Pilet, G.; Chastanet, G.; Luneau, D.; Ziessel, R. F.; Charbonnière, L. J.; Carrella, L.; Rentschler, E.; El Fallah, M., Syntheses, characterisation, magnetism and photoluminescence of a homodinuclear Ln (III)-Schiff base family. *Dalton Trans.* **2009,** (46), 10263-10272.

72. Guo, Y.-N.; Xu, G.-F.; Gamez, P.; Zhao, L.; Lin, S.-Y.; Deng, R.; Tang, J.; Zhang, H.-J., Two-step relaxation in a linear tetranuclear dysprosium (III) aggregate showing single-molecule magnet behavior. *J. Am. Chem. Soc.* **2010,** *132* (25), 8538-8539.
73. Shi, T.; Xu, Y.; Li, M.-X.; Liu, C.-M.; Nfor, E. N.; Wang, Z.-X., A 10-coordinate cerium (III) complex with a ferrocene-based terpyridine ligand exhibiting field-induced slow magnetic relaxation. *Polyhedron* **2020,** *188*, 114695.
74. Mautner, F. A.; Bierbaumer, F.; Fischer, R. C.; Tubau, A.; Speed, S.; Ruiz, E.; Massoud, S. S.; Vicente, R.; Gómez-Coca, S., Insights into the Spin Dynamics of Mononuclear Cerium (III) Single-Molecule Magnets. *Inorg. Chem.* **2022,** *61* (29), 11124-11136.
75. Leng, J.-D.; Hua, Q.-Y.; Liu, W.-T.; Tao, Z.-X.; Tan, N.-W.; Wang, Y.-F.; Lin, W.-Q., Slow magnetic relaxation of mononuclear complexes based on uncommon Kramers lanthanide ions Ce III, Sm III and Yb III. *Dalton Trans.* **2022**.